Construction and Building Materials 112 (2016) 1005–1012

Contents lists available at ScienceDirect

Construction and Building Materials

journal homepage: www.elsevier.com/locate/conbuildmat

Alkali-activated ground granulated blast-furnace slag incorporating incinerator fly ash as a potential binder

Yiquan Liu [a,b], Weiping Zhu [b], En-Hua Yang [b,*]

[a] Energy Research Institute @NTU (ERI@N), Interdisciplinary Graduate School, Nanyang Technological University, 50 Nanyang Avenue, Singapore 639798, Singapore
[b] School of Civil and Environmental Engineering, Nanyang Technological University, 50 Nanyang Avenue, Singapore 639798, Singapore

HIGHLIGHTS

- IFA was incorporated into alkali-activated GGBS binder as a construction material.
- IFA possesses lower cementing efficiency but shall not be considered as inert filler.
- Alkali-activated GGBS-IFA binders effectively immobilize leachable heavy metals.

ARTICLE INFO

Article history:
Received 25 September 2015
Received in revised form 28 January 2016
Accepted 22 February 2016
Available online 11 March 2016

Keywords:
Ground granulated blast-furnace slag (GGBS)
Alkali-activated
Incinerator fly ash (IFA)
Compressive strength
XRD
FTIR
Heavy metal leaching

ABSTRACT

Incinerator fly ash (IFA) is the ash residual after incineration of municipal solid waste. Due to the presence of more leachable trace elements, utilization of IFA is rare. Alkali-activated GGBS has been report to possess superior heavy metal immobilization capability. This study investigated the influence of IFA addition on the mechanical strength, chemical structure, and heavy metal leaching of alkali-activated GGBS-IFA binders. It revealed that the IFA used in this study is less reactive than GGBS and has a low efficiency factor of 0.13 due to high crystallinity and low Si and Al content. Incorporation of IFA hinders the formation of gel and reduces the compressive strength of the resulting alkali-activated GGBS-IFA binder. However, even at high IFA content where 60% of GGBS was replaced by IFA, a moderate compressive strength of around 17 MPa of the resulting binder can still be obtained. Alkali-activated GGBS-IFA binders provided effective means to immobilize heavy metals. The incorporation of IFA into alkali-activated GGBS binders provides a possible measure to utilize IFA as construction materials for civil engineering applications.

1. Introduction

Cement production consumes huge amount of raw materials and energy (3100–3600 kJ/kg) [1] and is not environmental friendly. Production of one ton of cement liberates about equal amount of greenhouse gases into the atmosphere [2]. The annual worldwide production of cement generates about 1.35 billion tons of greenhouse gases, which contributes to around 7% of the total global greenhouse gas generation [3]. In light of these problems, in recent years, there has been a growing interest in the community to develop cementless binders for construction industry. For example, Popescu et al. [1] worked on industrial trial production of belite cement. Yang et al. [4] developed cementless mortars activated by sodium silicate. Davidovits [5] invented geopolymer binders.

Ground granulated blast-furnace slag (GGBS) is a by-product from the iron manufacturing industry. Alkali-activated GGBS has been extensively studied as an alternative binder. Douglas [6,7] made a preliminary study on alkali-activated GGBS. Song et al. [8] studied the hydration of alkali-activated GGBS. Want et al. [9] studied the factors which affect the strength of alkali-activated slag. They also summarized that alkali-activated GGBS has advantages over ordinary Portland cement (OPC) such as rapid strength gain, high strength, good durability and high resistance to chemical attack [10]. It has also been reported recently about the possibility of blending other industrial by-product or waste into alkali-activated GGBS matrix to create cementless binder. Yusuf et al. [11] blended GGBS with ultrafine palm oil fuel ash to synthesize a new binder which achieved higher compressive strength than that of OPC-based binder. Rashad et al. [12] mixed alkali-activated GGBS with silica fume, a by-product from the production

* Corresponding author at: N1-01b-56, 50 Nanyang Avenue, Singapore 639798, Singapore.
E-mail address: ehyang@ntu.edu.sg (E.-H. Yang).

http://dx.doi.org/10.1016/j.conbuildmat.2016.02.153
0950-0618/

of metallic silicon or ferrosilicon alloys. The result showed that the replacement of GGBS with silica fume up to 15% improved the compressive strength. Cho et al. [13] incorporated dredged sediment waste into alkali-activated GGBS and demonstrated the potential to be used as construction material. Coal fly ash can also be incorporated into alkali-activated GGBS [14] and researchers have conducted detailed investigation on the hydration products [15], mechanical strength [16], and microstructure [17] of alkali-activated GGBS/coal fly ash binder system. It was also found alkali-activated GGBS has superior heavy metal immobilization capability due to chemical bonding of binder and/or lower matrix porosity [18,19] and may be used for waste solidification treatment which is of great benefit to the environment [20].

With economic development and population increase, municipal solid waste (MSW) has increased tremendously over the years. Incineration significantly reduces the volume of MSW by 90% [21]. The residual ash, however, still needs to be disposed of, normally by landfill. Utilization of incinerator ash to deviate it from landfill and to prolong the lifespan of landfill is of great importance for cities or countries like Singapore where limited land space constrain the expansion of landfill. There are two types of incinerator ash, i.e. incinerator fly ash (IFA) and incinerator bottom ash (IBA). IBA can be used as average quality aggregate [22] for road construction [23,24]. Very few study; however, reported potential utilization of IFA due to high toxicity and the presence of more leachable trace elements. For example, Gao et al. [39] reported the use of IFA as partial cement replacement in mortars and showed high heavy metal leaching from the resulting IFA cement mortar. Heavy metal immobilization of IFA; therefore, is of great concern and importance for any potential utilization and application of IFA.

To our knowledge, there is no previous study on alkali-activated GGBS incorporating IFA. This paper investigated the combined use of GGBS and IFA as raw materials to synthesize alkali-activated GGBS-IFA binder. Physical properties and chemical compositions of the raw ingredients, the mechanical properties, the chemical composition, and nano-structure of the resulting GGBS-IFA binder, as well as heavy metal leaching of IFA and GGBS-IFA binder were evaluated and reported in this paper.

2. Experimental program

2.1. Raw materials

Fine GGBS (P8000) with a Blaine fineness of 870 m^2/kg was used in this study. The specific gravity and the bulk density of said GGBS are 2.9 and 1 mt/m^3, respectively. IFA was collected from Keppel Seghers Tuas Waste-to-Energy Plant. It is Singapore's fifth incineration plant and is able to treat 800 tons of solid waste daily to generate about 22 MW of green energy. The particle size distribution of GGBS and IFA determined by the laser particle size analyser is shown in Fig. 1. The average particle size of IFA is about 40 μm and 90% of IFA particles are smaller than 200 μm. Compared to IFA, the GGBS particles are much smaller with an average particle size of 13 μm and 90% of GGBS particles are smaller than 40 μm.

The chemical composition of the major elements in GGBS and IFA was determined by X-ray Fluorescence Spectroscopy (XRF) and the results are shown in Table 1. The GGBS has high amount of SiO_2 and Al_2O_3 and the IFA used in this study has very low alumina and silica content. Both IFA and GGBS consist of high amount of CaO.

2.2. Mix design and processing

Mix proportions of alkali-activated GGBS-IFA were summarized in Table 2. The alkaline solution was a mixture of 20 g of sodium hydroxide, 40 g of sodium silicate with the molar ratio of SiO_2 to Na_2O of 2.9 to 3.2, and 90 g of water. Mixing, casting, and curing are done as follows: (a) GGBS and IFA were dry-mixed for 3 min in a table top mixer, (b) the alkaline solution was slowly added into the mix and mixed for another three minutes until a homogenous and consistent paste was achieved, (c) the fresh paste was poured into 50 mm cubic moulds and vibrated for 30 s, (d) the surface of moulds was covered by plastic sheet to prevent water evaporation, and (e) the specimens were cured in an oven at temperature of 75 °C for 3 days before testing. Few samples were cured in the same condition for 7 days for additional FTIR tests.

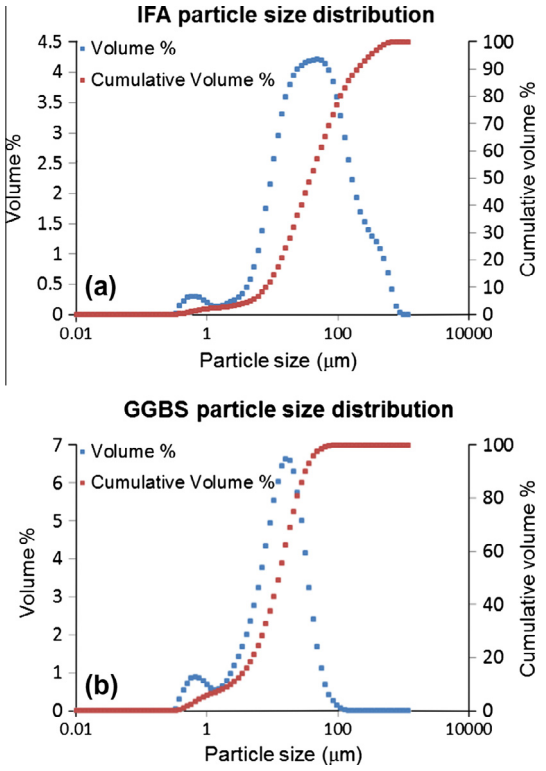

Fig. 1. Particle size distribution of (a) IFA powder and (b) GGBS powder used in this study.

2.3. Tests

After 3 days of curing, compressive test was conducted according to ASTM standard C109 to reveal the compressive strength of alkali-activated GGBS-IFA binder. At least three samples of each mix were tested and the average was reported as the nominal compressive strength. X-ray powder diffraction (XRD) and Fourier transform infrared spectroscopy (FTIR) were used to quantify the chemical composition and structure of alkali-activated GGBS-IFA binder.

To evaluate leaching of heavy metals from the resulting alkali-activated GGBS-IFA binders, leaching tests of monolithic material according to the EA NEN 7375 standard were carried out. In this test, the moulded specimen of defined geometry (50 mm cube) was immersed in a predetermined container filled with deionized water. The volume of water should be approximately 5 times that of the specimen and the thickness of water surrounding the surfaces of the specimen should be at least 20 mm. Leaching solutions were exchanged with fresh deionized water at predetermined cumulative time intervals of 0.25, 1, 2.25, 4, 9, 16, 36 and 64 days. The eluate was filtered through a 0.45 μm polypropylene filtration membrane. The concentration of different trace metals in eluate was determined by means of inductively coupled plasma atomic emission spectroscopy (ICP-OES). The results were used to calculate "measured leaching of a component per fraction" and "measured cumulative leaching" based on the formulas from EA NEN 7375 as follows.

Measured leaching of a component per fraction

$$E_i^* = \frac{C_i \times V}{f \times A} \quad (1)$$

where

E_i^* is the measured leaching of a component in fraction i in mg/m^2;
C_i is the concentration of the component in fraction i in μg/l;
V is the volume of the eluate in l;
A is the surface area of the test piece in m^2; and
f = 1000 μg/mg is a conversion factor.

Measured cumulative leaching

$$\varepsilon_n^* = \sum_{i=1}^{n} E_i^* \quad for\ n = 1\ to\ N \quad (2)$$

where

ε_n^* is the measured cumulative leaching of a component for period n comprising fraction; E_i^* is the measured leaching of the component in fraction i in mg/m^2; i = 1 to n in mg/m^2; and
N is the number of periods equal to the number of specified replenishment times (N = 8).

Table 1
Chemical compositions of GGBS and IFA.

Oxides	CaO	SiO_2	Al_2O_3	MgO	SO_3	TiO_2	K_2O	Fe_2O_3	Na_2O	MnO	ZnO	P_2O_5	Cl
GGBS (%)	39.43	31.19	13.41	9.32	4.25	0.66	0.53	0.38	0.33	0.29	–	–	–
IFA (%)	47.37	2.24	1.03	1.64	5.29	0.75	6.69	0.81	4.89	0.06	2.49	0.72	25.03

Table 2
Mix proportion of alkali-activated GGBS-IFA binders.

Mix No.	GGBS (g)	IFA (g)	NaOH (g)	Sodium silicate (g)	Water (g)	Effective binder (GGBS + k IFA)	Water-to-effective binder ratio
1	100	0	20	40	90	100	0.9
2	97	3	20	40	90	97.4	0.92
3	95	5	20	40	90	95.6	0.94
4	90	10	20	40	90	91.3	0.99
5	80	20	20	40	90	82.6	1.09
6	60	40	20	40	90	65.2	1.38
7	40	60	20	40	90	47.8	1.89
8	0	100	20	40	90	12.9	6.98

To evaluate the potential release of heavy metals from IFA powder, leaching tests of pulverized material according to EN 12457-2 standard were carried out. The leaching test was performed at a liquid-to-solid ratio of 10 L/kg and deionized water was used as leachant. The eluate from the leaching tests was filtered through a 0.45 μm polypropylene filtration membrane. The concentration of different trace metals in eluate was determined by means of ICP-OES. The as-obtained concentration of heavy metal in eluate is multiplied by the volume of eluate to get the total mass of heavy metal in eluate. This number was then divided by the mass of IFA used for the leaching test to get the leaching of heavy metals from IFA with the unit of mg/kg.

3. Results and discussion

3.1. Compressive strength of alkali-activated GGBS-IFA binder

Fig. 2 shows compressive strength of alkali-activated GGBS-IFA binder. The compressive strength reduces with increasing IFA content indicating IFA is less reactive than GGBS subject to alkaline activation. The cementing efficiency of IFA can be calculated based on the measured compressive strength. The efficiency factory (k-value) of IFA is defined as the number of parts of GGBS that could be replace by one part of IFA without changing the compressive strength of the resulting binder. Since the compressive strength of pure GGBS binder and pure IFA binder is 39 MPa and 5 MPa, respectively, the k-value of IFA is 5/39 = 0.13, i.e. 1 kg of IFA is equivalent to 0.13 kg of GGBS.

Table 2 summarizes the effective binder (GGBS + k IFA) and the water-to-effective binder ratio of GGBS-IFA mixes. Fig. 3 plots the compressive strength of the alkali-activated GGBS-IFA binder as a function of the water-to-effective binder ratio. The compressive strength is inversely proportional to the water-to-effective binder ratio similar to the Abrams' law, which linearly relates the logarithm of strength of cement paste to the water-to-cement ratio. This may suggest that the microstructure of the alkali-activated GGBS-IFA binder is similar to C—S—H or modified C—S—H such as C—(N, A)—S—H.

3.2. XRD analysis

XRD spectra reveal the crystal structure of GGBS powder and IFA powder as shown in Figs. 4 and 5, respectively. As can be seen, very few crystal phases and a broad hump between (2θ) 25° and 35° are observed in the GGBS spectrum which suggests GGBS mainly consists of amorphous calcium aluminum silicate and is in metastable state. IFA, on the other hand, contains many crystalline phases including metal chloride, calcium carbonate and calcium sulfate. This makes IFA a potentially low reactivity material and is unfavorable for the alkaline activation as compared to GGBS. However, IFA should not be considered as inert filler since a 5 MPa compressive strength was recorded for samples made from 100% IFA.

Fig. 4 compares the XRD spectra of GGBS powder and alkali-activated GGBS binder (Mix 1). It shows that GGBS consists of a broad hump of amorphous calcium aluminum silicate with few crystal aluminum oxide and calcium aluminum silicate peaks. After alkaline activation, the aluminum oxide peaks disappears and new C—S—H peaks are identified in the alkali-activated GGBS binder.

Fig. 5 compares the XRD spectra of IFA powder and alkali-activated IFA binder (Mix 8). It shows that IFA contains much more crystalline phases including metal chloride, calcium carbonate and calcium sulfate. After alkaline activation, the calcium sulfate peak disappears and new C—S—H phase $Ca_6Si_6O_{17}(OH)_2$ and $Ca_6(SiO_3)_6$·H_2O are generated in the alkali-activated IFA binder. This is perhaps due to the reaction of the soluble calcium ions from IFA and the silicate ions from the alkaline solution as shown in the following equations:

$$6Ca^{2+} + 6SiO_3^{2-} + H_2O \rightarrow Ca_6Si_6O_{17}(OH)_2 \quad (3)$$

$$6Ca^{2+} + 6SiO_3^{2-} + H_2O \rightarrow Ca_6(SiO_3)_6 \cdot H_2O \quad (4)$$

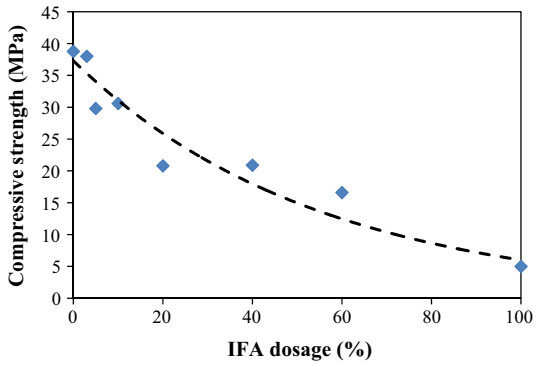

Fig. 2. Effect of IFA dosage on the compressive strength of alkali-activated GGBS-IFA binder.

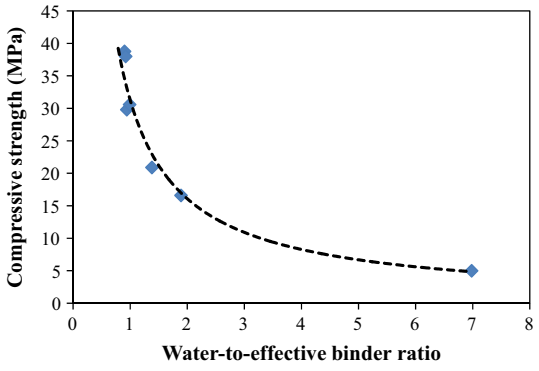

Fig. 3. Compressive strength of alkali-activated GGBS-IFA binder as a function of water-to-effective binder ratio.

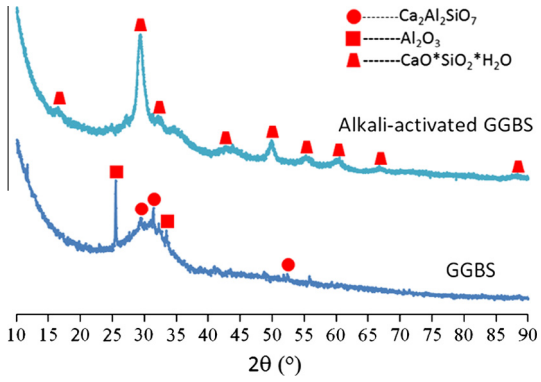

Fig. 4. XRD spectra of GGBS powder and alkali-activated GGBS binder (Mix 1).

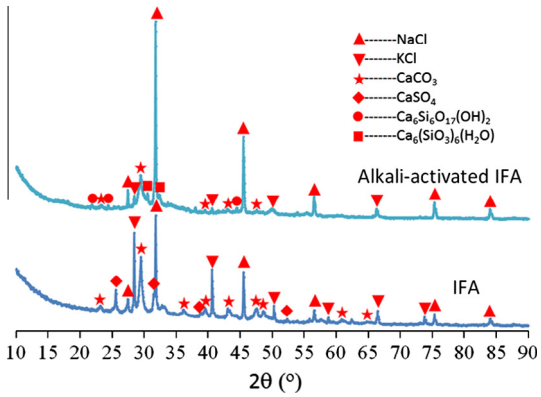

Fig. 5. XRD spectra of IFA powder and alkali-activated IFA binder (Mix 8).

Fig. 6 shows the XRD spectra of alkali-activated GGBS-IFA binders with 20% and 60% IFA (Mixes 5 and 7). As can be seen, the main phases in alkali-activated GGBS-IFA binders are calcium carbonate and calcium silicate hydrate. The general trend shows that the C—S—H peaks reduce while the calcium carbonate peaks increase with increase of IFA dosage. This suggests the inclusion of IFA undermines the alkali-activated hydration reaction of GGBS and brings in more crystal calcium carbonate.

3.3. FTIR analysis

Fig. 7 shows the FTIR spectra of GGBS powder and alkali-activated GGBS binders (Mix 1) cured for 3-day and 7-day. Wavenumber range of 800–1200 cm^{-1} is characteristic of Si—O—Si(Al) [25]. In GGBS powder, broad peak around 960 cm^{-1} represents the asymmetric stretching band of Si—O—Si and Al—O—Si [26], and peak around 460 cm^{-1} is the bending vibration of Si—O—Si bonds [27]. Peak at around 680 cm^{-1} is the S—O bending band of sulfates [28]. Significant change in FTIR spectrum is observed after alkali-activation as shown in Fig. 7. Overall, the broad peak centered around 960 cm^{-1} in spectrum of GGBS powder narrows to a much sharper peak around 991 cm^{-1} in spectra of alkali-activated GGBS. This implies more Si(Al) tetrahedrons had been incorporated into the binder system and chain lengths had increased, as peak shifting upward indicates more polymerized Si—O—Si(Al) structure [29]. The shape and the intensity of the 7-day FTIR spectrum remain similar to that of the 3-day results. Unlike ordinary Portland cement in which hydration takes months to years to be fully developed, reaction of alkaline activation is very fast. Therefore, the samples used for the following FTIR analysis were all 3-day cured samples.

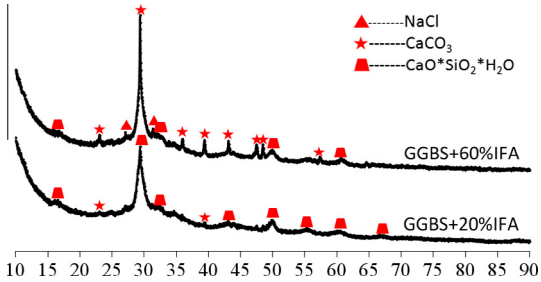

Fig. 6. XRD spectra of alkali-activated GGBS-IFA binder with 20% (Mix 5) or 60% (Mix 7) IFA.

Fig. 8 shows the FTIR spectra of IFA powder and alkali-activated IFA sample (Mix 8). In the spectrum of IFA powder, no apparent peaks around 1000 and 460 cm^{-1} which are characteristic absorptions of Si tetrahedron, though a Q4 peak at around 1156 cm^{-1} was observed. New peaks related to asymmetric stretching of Si—O—Si (Al) at 960 cm^{-1} and bending vibration of Si—O—Si at 457 cm^{-1} appear in the spectrum of alkali-activated IFA. This indicates formation of Si—O—Si(Al) bonds, i.e. gel, after alkaline activation of IFA which is similar to the alkaline activation of GGBS to some extent. The peak at 874 cm^{-1}, which is enhanced from IFA to alkali-activated transformation, belongs to out plane bending of carbonates [25]. The peak at 674 cm^{-1} in spectrum of IFA is due to the S-O bending of sulfates [28].

Fig. 9 compares FTIR spectra of alkali-activated GGBS-IFA binders with 0%, 20%, 60% and 100% IFA (Mixes 1, 5, 7, and 8). The peaks at around 1000 cm^{-1} are Si—O—Si(Al) bonds formed after alkaline activation, i.e. gel. It can be seen that the height and area of the peaks at around 1000 cm^{-1} reduce with increase of IFA dosage. According to Beer–Lambert law, intensity of absorbance is proportional to the concentration [30]. This suggests that the quantity of gels in alkali-activated GGBS-IFA binders reduces with increasing IFA dosage, which explains reduced compressive strength of the alkali-activated GGBS-IFA with increase of IFA dosage in Fig. 2. The reduced gel content with increase of IFA dosage is a result of less active Si and Al content in IFA.

Deconvolution of FTIR spectra was carried out to reveal individual peaks in the broad band of 800–1200 cm^{-1} due to overlapping of peaks. The locations of peaks were identified by taking second derivative of the original spectrum, and the shapes of all peaks were assumed to follow Gaussian function [31]. The deconvoluted alkali-activated GGBS (Mix 1) spectrum and the alkali-activated IFA (Mix 8) spectrum are shown as examples in Fig. 10, where

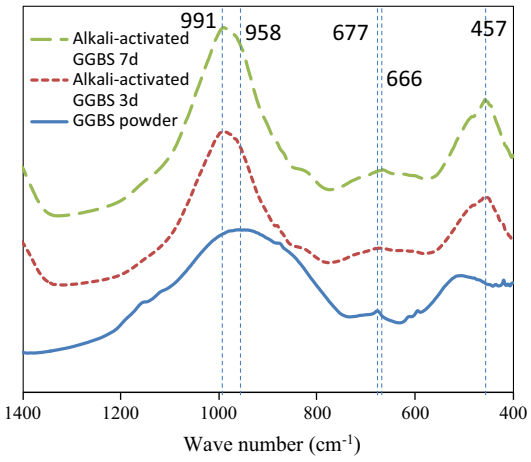

Fig. 7. FTIR spectra of GGBS powder and alkali-activated GGBS binder (Mix 1).

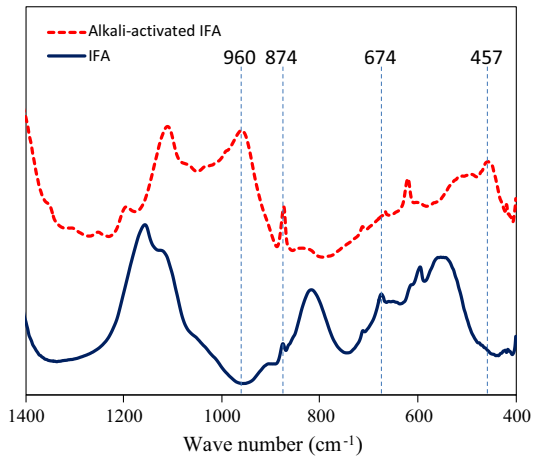

Fig. 8. FTIR spectra of IFA powder and alkali-activated IFA binder (Mix 8).

black curves are the original spectra, green curves are individual peaks identified after deconvolution, and red curves are the cumulative result of individual peaks. Similarly, spectra of GGBS powder, IFA powder, and alkali-activated GGBS-IFA binder with 20% and 60% IFA were deconvoluted and the results are summarized in Table 3. Values in parentheses are proportions of individual peak area to the total area in the range of 800–1200 cm^{-1}. As can be seen, most of the identified peaks are associated with Si—O—Si (Al) vibrations according to FTIR library from literature [25,27,31–35].

From Table 3, comparing the spectra of alkali-activated GGBS (Mix 1) with GGBS powder, newly formed Q2 (982 cm^{-1}) peak, i.e. gel, is the dominant phase which accounts for 78.1% of the total Si—O—Si(Al) bonds in the alkali-activated GGBS. The small percentage of Q1 (827 cm^{-1}) peak suggests longer Q2 Si—O—Si(Al) chain formed in the alkali-activated GGBS, probably due to thermal curing of the sample. Some Q3 Si—O—Si(Al) bonds exist in both the GGBS and the alkali-activated GGBS indicating incomplete reaction of GGBS particles even after alkali activation. Comparing alkali-activated IFA (Mix 8) with IFA powder, Q1 (818 cm^{-1}) and Q4 (1156 cm^{-1}) peaks in IFA disappear while three dominant peaks at Q2 (953 cm^{-1} [23.6%] and 1001 cm^{-1} [21.1%]) and Q3 (1112 cm^{-1} [35.4%]) appear in the alkali-activated IFA, which means Si—O bonds in IFA experience dissolution, reorganization and eventually polymerization. Comparing alkali-activated GGBS-IFA samples, percentage of Q2 (~980 cm^{-1}), i.e. newly formed gel, is reduced from 78.1% (0% IFA) to 47.5% (20% IFA) and to

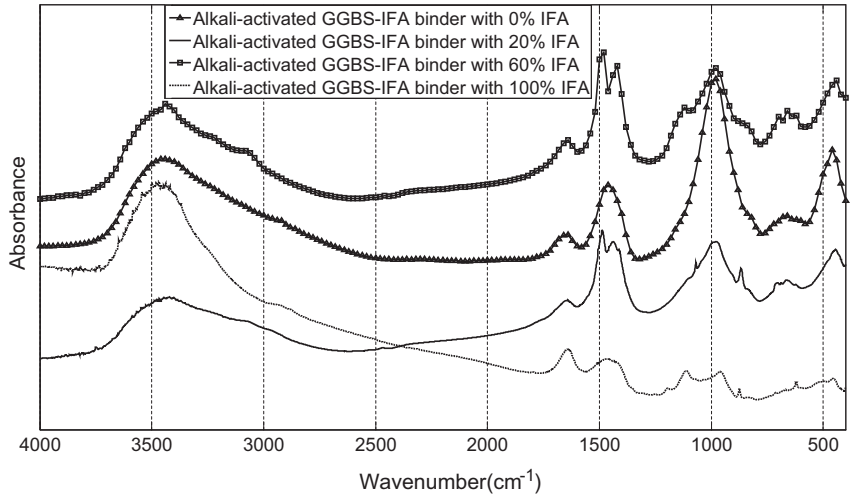

Fig. 9. FTIR spectra of alkali-activated GGBS-IFA binder with 0% (Mix 1), 20% (Mix 5), 60% (Mix 7) and 100% (Mix 8) IFA.

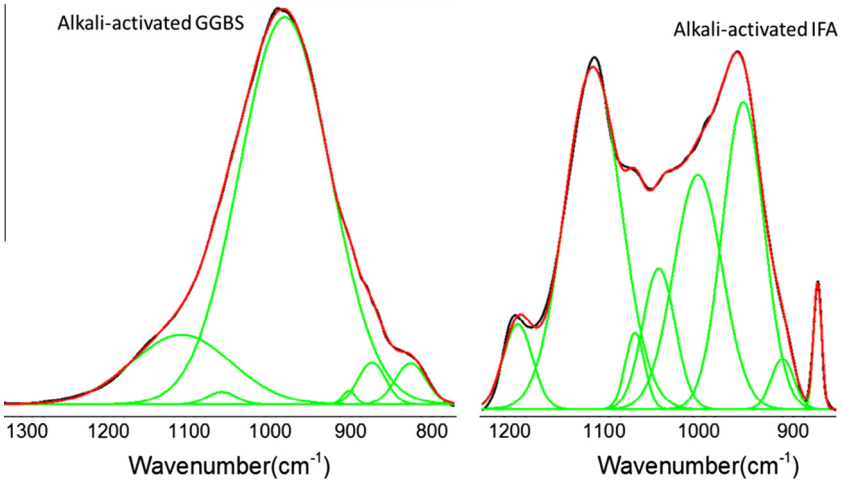

Fig. 10. Deconvoluted FTIR spectra of alkali-activated GGBS (Mix 1) and alkali-activated IFA (Mix 8).

Table 3
Deconvolution of FTIR spectra between 800 and 1200 cm^{-1}.

Peak location (Area%)	Si—O (Q1)	C—O	Si—O	Si—O	Si—O (Q2)	Si—O	Si—O	Si—O	Si—O (Q3)	Si—O (Q4)	Si—O
GGBS powder	817 (6.3%)	860 (9.9%)		924 (29.9%)		997 (20.6%)	1051 (4.5%)		1109 (27.2%)		
IFA powder	818 (20.6%)	875 (1.5%)	908 (1.9%)				1051 (12.5%)			1156 (58.5%)	
Alkali-activated GGBS-IFA (Mix 1, 0% IFA)	827 (2.8%)	875 (2.6%)	903 (0.4%)		982 (78.1%)		1060 (0.8%)		1110 (15.3%)		
Alkali-activated GGBS-IFA (Mix 5, 20% IFA)	838 (4.8%)	867 (3.4%)	899 (6.1%)		978 (47.5%)		1046 (1.0%)	1069 (0.5%)	1085 (36.6%)		
Alkali-activated GGBS-IFA (Mix 7, 60% IFA)	836 (5.4%)	871 (3.0%)	907 (4.7%)		974 (42.5%)		1050 (20.8%)	1069 (0.8%)	1114 (1.4%)	1139 (21.3%)	
Alkali-activated GGBS-IFA (Mix 8, 100% IFA)		874 (1.9%)	911 (2.1%)		953 (23.6%)	1001 (21.1%)	1042 (8.5%)	1068 (2.8%)	1112 (35.4%)		1192 (4.6%)

42.5% (60% IFA). The addition of IFA hinders the formation of Q2 (~980 cm^{-1}) which is consistent with the observation of reduced compressive strength of the alkali-activated GGBS-IFA with increasing IFA dosage as shown in Fig. 2. In addition, it seems that Q2 peak shifts towards lower wavenumber with the addition of IFA.

3.4. Leaching analysis

Heavy metal leaching of IFA powder according to EN 12457-2 for pulverized material and corresponding limits established by European Union Landfill Directive (EULFD) for the acceptance of waste landfills are given in Table 4. As can be seen, the IFA used in this study cannot be landfilled directly as few trace elements including As, Pb and Zn exceed the limiting value of non-hazardous landfill. The concentration in leachates for Pb in particular is much higher than the EULFD limits for hazardous landfill. Therefore, IFA needs to be treated for heavy metal immobilization before it can be landfilled.

The 64-day cumulative leaching of heavy metals of alkali-activated GGBS-IFA binder according to EA NEN 7375 tank leaching for monolithic material and corresponding limits established by Decree on Soil Quality (DSQ, the successor of the Dutch Building Material Decree) for the acceptance of materials (primary, secondary and waste) used in construction [36–38] are summarized in Table 5. It shows that the leaching of heavy metals increases with increase of IFA content. Even at very high IFA, the concentrations of all trace elements in leachate are however still much lower than the DSQ limits for moulded building materials. This suggests that the alkali-activated GGBS-IFA can be a potential binder for construction applications.

Fig. 11 shows the cumulative leaching of the major heavy metal As, Cd, Pb and Zn of the alkali-activated GGBS-IFA samples. The general trend shows that the cumulative concentration increases with time. However, the rate of leaching reduces significantly and stabilizes after 400 h. Therefore, alkali-activated GGBS is an effective way to immobilize heavy metals in IFA. The incorporation of IFA into alkali-activated GGBS provides a possible measure to utilize IFA as construction material for civil engineering applications.

Table 4
Heavy metal leaching of IFA powder according to EN 12457-2 for pulverized material and EULFD limits for the acceptance of waste landfills (mg/kg dry mass).

Elements	Concentrations in leachates	EULFD limits		
		Inert	Non-hazardous	Hazardous
As	3.2	0.5	2	25
Cd	0.01	0.04	1	5
Cr	2.41	0.5	10	70
Cu	6.84	2	50	100
Ni	0.09	0.4	10	40
Pb	779.8	0.5	10	50
Zn	128.3	4	50	200

Table 5
64-day cumulative leaching of heavy metals from alkali-activated GGBS-IFA binder according to EA NEN 7375 for monolithic material and DSQ limits for the acceptance of materials used in construction (mg/m^2).

Element	Concentration in leachate GGBS:IFA			DSQ limits for moulded building materials
	80:20	60:40	40:60	
As	19.04	36.21	52.87	260
Cd	0.93	1.49	2.43	3.8
Cr	0.28	0.93	1.73	120
Cu	4.11	4.57	4.06	98
Ni	0.05	0.05	0.09	81
Pb	7.89	19.04	22.21	400
Zn	32.67	66.03	121.47	800

4. Conclusions

This paper evaluates the influence of incinerator fly ash (IFA) on the mechanical strength, microstructure, and leaching of the resulting alkali-activated GGBS-IFA binder. XRD and FTIR tests were used to reveal the chemical structure of the binder and the Q structure transformations during the reaction process.

Due to high crystallinity of IFA used in this study, the incorporation of IFA reduces the compressive strength of alkali-activated GGBS-IFA binder. However, IFA shall not be considered as inert filler as 5 MPa compressive strength can be obtained for samples made from 100% IFA. This suggests IFA is less reactive than GGBS with a low efficiency factor k of 0.13 in producing alkali-activated GGBS-IFA binder.

The formation of new Q2 and Q3 peaks in the alkali-activated GGBS-IFA suggests Si—O bonds in the GGBS-IFA mixes still experience dissolution, reorganization and eventually polymerization, i.e. gel formation. However, the intensity and area proportion of these peaks reduce with the increase of IFA dosage which suggests IFA hinders the formation of gel and causes reduced strength of the alkali-activated GGBS-IFA binder.

Alkali-activated GGBS-IFA binder provides an effective means to immobilize heavy metals in the system even at high IFA content where 60% of GGBS is replaced by IFA and a moderate compressive strength of ~17 MPa of the resulting binder can be obtained. The incorporation of IFA into alkali-activated GGBS provides a possible measure to utilize IFA as construction material for civil engineering applications.

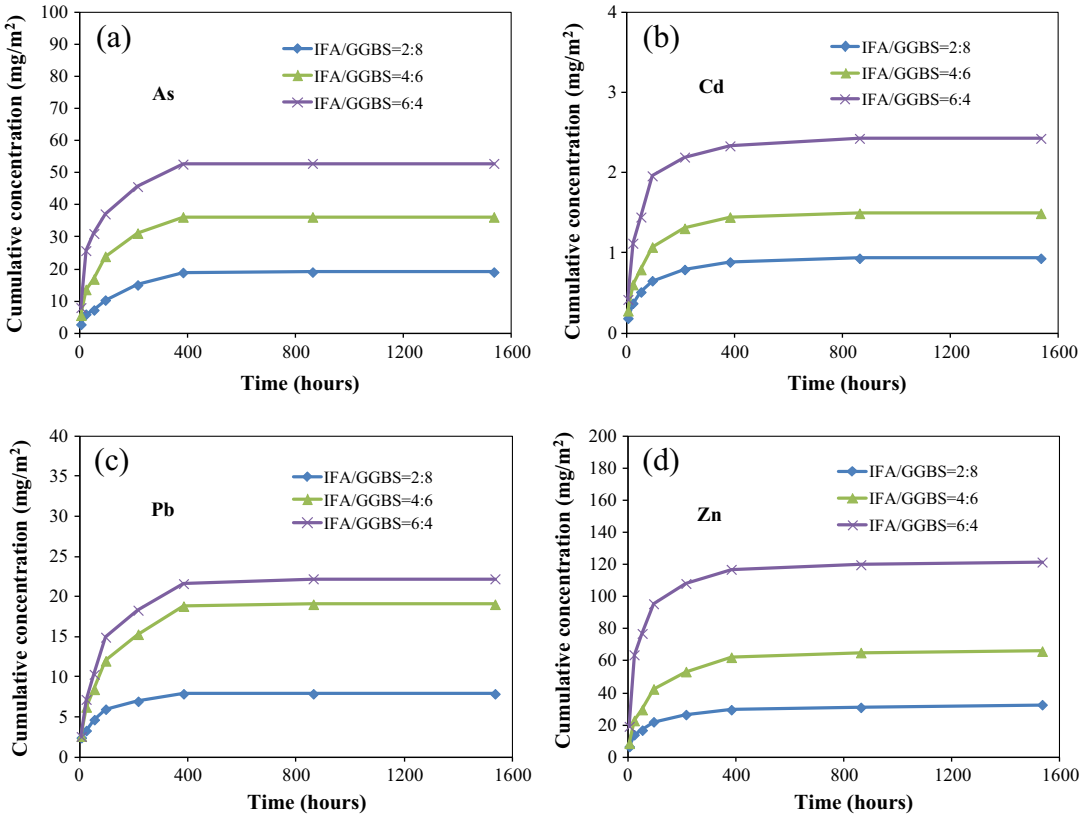

Fig. 11. Cumulative leaching of the major heavy metal (a) As, (b) Cd, (c) Pb and (d) Zn of alkali-activated GGBS-IFA binders.

Acknowledgment

The financial support from the Republic of Singapore's National Research Foundation through a grant to the Berkeley Education Alliance for Research in Singapore (BEARS) for the Singapore-Berkeley Building Efficiency and Sustainability in the Tropics (Sin-BerBEST) program is gratefully acknowledged.

References

[1] C.D. Popescu, M. Muntean, J.H. Sharp, Industrial trial production of low energy belite cement, Cem. Concr. Compos. 25 (2003) 689–693.
[2] Djwantoro Hardjito, Studies of Fly Ash-based Geopolymer Concrete, Curtin University of Technology, 2005.
[3] V.M. Malhotra, Introduction: sustainable development and concrete technology, Concr. Int. 24 (2002) 22.
[4] Keun-Hyeok Yang, Jin-Kyu Song, Ashraf F. Ashour, Eun-Taik Lee, Properties of cementless mortars activated by sodium silicate, Constr. Build. Mater. 22 (2008) 1981–1989.
[5] J. Davidovits, Geopolymer chemistry and properties, Geopolymer 88 (1988) 25–48.
[6] E. Douglas, J. Brandstetr, A preliminary study on the alkali activation of ground granulated blast-furnace slag, Cem. Concr. Res. 20 (1990) 746–756.
[7] E. Douglas, A. Bilodeau, J. Brandstetr, V.M. Malhotra, Alkali activated ground granulated blast-furnace slag concrete: preliminary investigation, Cem. Concr. Res. 21 (1991) 101–108.
[8] S. Song, D. Sohn, H.M. Jennings, T.O. Mason, Hydration of alkali-activated ground granulated blast furnace slag, J. Mater. Sci. 35 (2000) 249–257.
[9] Shao-Dong Wang, Karen L. Scrivener, P.L. Pratt, Factors affecting the strength of alkali-activated slag, Cem. Concr. Res. 24 (1994) 1033–1043.
[10] Shao-Dong Wang, Xin-Cheng Pu, K.L. Scrivener, P.L. Pratt, Alkali-activated slag cement and concrete: a review of properties and problems, Adv. Cem. Res. 7 (1995) 93–102.
[11] Moruf Olalekan Yusuf, Megat Azmi Megat Johari, Zainal Arifin Ahmad, Mohammad Maslehuddin, Evolution of alkaline activated ground blast furnace slag–ultrafine palm oil fuel ash based concrete, Mater. Design 55 (2014) 387–393.
[12] Alaa M. Rashad, Mervat H. Khalil, A preliminary study of alkali-activated slag blended with silica fume under the effect of thermal loads and thermal shock cycles, Constr. Build. Mater. 40 (2013) 522–532.
[13] Han-na Cho, Jae-Ho Shim, Joo-Yang Park, Performance evaluation of solidification/stabilization of dredged sediment using alkali-activated slag, Desalin Water Treat (2015) 1–10 (ahead-of-print).
[14] Sundara Raman Chithiraputhiran, Kinetics of Alkaline Activation of Slag and Fly ash-Slag Systems PhD diss., Arizona State University, 2012.
[15] F. Puertas, S. Martínez-Ramírez, S. Alonso, T. Vazquez, Alkali-activated fly ash/slag cements: strength behaviour and hydration products, Cem. Concr. Res. 30 (2000) 1625–1632.
[16] C. Shi, R.L. Day, Early strength development and hydration of alkali-activated blast furnace slag/fly ash blends, Adv. Cem. Res. 11 (1999) 189–196.
[17] F. Puertas, A. Fernández-Jiménez, Mineralogical and microstructural characterisation of alkali-activated fly ash/slag pastes, Cem. Concr. Compos. 25 (2003) 287–292.
[18] Jan. Deja, Immobilization of Cr^{6+}, Cd^{2+}, Zn^{2+} and Pb^{2+} in alkali-activated slag binders, Cem. Concr. Res. 32 (2002) 1971–1979.
[19] Caijun Shi, A. Fernandez-Jimenez, Stabilization/solidification of hazardous and radioactive wastes with alkali-activated cements, J. Hazard. Mater. 137 (2006) 1656–1663.
[20] J. Malolepszy, J. Deja, Immobilization of heavy metal ions by the alkali activated slag cementitious materials, Stud. Environ. Sci. 60 (1994) 519–524.
[21] J.L. Ontiveros, T.L. Clapp, D.S. Kosson, Physical properties and chemical species distributions within municipal waste combuster ashes, Environ. Prog. 8 (1989) 200–206.
[22] J. Pera, L. Coutaz, J. Ambroise, M. Chababbet, Use of incinerator bottom ash in concrete, Cem. Concr. Res. 27 (1997) 1–5.
[23] R. Forteza, M. Far, C. Seguí, V. Cerda, Characterization of bottom ash in municipal solid waste incinerators for its use in road base, Waste Manage. 24 (2004) 899–909.
[24] Maria Izquierdo, Enric Vazquez, Xavier Querol, Marilda Barra, Angel Lopez, Felicià Plana, Use of bottom ash from municipal solid waste incineration as a road material, in: International Ash Utilization Symposium, Lexington, KY, United States, 2001, pp. 31–38.
[25] I. Lecomte, Catherine Henrist, M. Liegeois, F. Maseri, André Rulmont, Rudi Cloots, (Micro)-structural comparison between geopolymers, alkali-activated slag cement and Portland cement, J. Eur. Ceram. Soc. 26 (2006) 3789–3797.
[26] W.K.W. Lee, JS J. van Deventer, Effects of anions on the formation of aluminosilicate gel in geopolymers, Ind. Eng. Chem. Res. 41 (2002) 4550–4558.
[27] M. Mollah, A. Yousuf, Felix Lu, David L. Cocke, An X-ray diffraction (XRD) and Fourier transform infrared spectroscopic (FT-IR) characterization of the speciation of arsenic (V) in Portland cement type-V, Sci. Total Environ. 224 (1998) 57–68.
[28] Ena Smidt, Katharina Böhm, Manfred Schwanninger, The Application of FT-IR Spectroscopy in Waste Management, Intech Open Access Publisher, 2011.

[29] M. Criado, Ana Fernández-Jiménez, A. Palomo, Alkali activation of fly ash: effect of the SiO_2/Na_2O ratio: Part I: FTIR study, Microporous Mesoporous Mater. 106 (2007) 180–191.
[30] J.D. Ingle Jr., S.R. Crouch, Spectrochemical Analysis, Prentice Hall, New Jersey, 1988.
[31] Kim N. Dalby, Penelope L. King, A new approach to determine and quantify structural units in silicate glasses using micro-reflectance Fourier-Transform infrared spectroscopy, Am. Mineral. 91 (2006) 1783–1793.
[32] R.A. Hanna, P.J. Barrie, C.R. Cheeseman, C.D. Hills, P.M. Buchler, R. Perry, Solid state ^{29}Si and ^{27}Al NMR and FTIR study of cement pastes containing industrial wastes and organics, Cem. Concr. Res. 25 (1995) 1435–1444.
[33] Ping Yu, R. James Kirkpatrick, Brent Poe, Paul F. McMillan, Xiandong Cong, Structure of calcium silicate hydrate (C–S–H): Near-, Mid-, and Far-infrared spectroscopy, J. Am. Ceram. Soc. 82 (1999) 742–748.
[34] N. Clayden, S. Esposito, A. Aronne, P. Pernice, Solid state ^{27}Al NMR and FTIR study of lanthanum aluminosilicate glasses, J. Non-Cryst. Solids 258 (1999) 11–19.
[35] I. García-Lodeiro, A. Fernández-Jiménez, M.T. Blanco, A. Palomo, FTIR study of the sol–gel synthesis of cementitious gels: C-S–H and N–A–S–H, J. Sol-Gel. Sci. Technol. 45 (2008) 63–72.
[36] Decree on Soil Quality. Staatsblad 2007. Besluit van 22 november 2007, houdende regels inzake de kwaliteit van de bodem (Besluit bodemkwaliteit). Staatsblad, 2007, nr 469.
[37] Carlos Leiva, C. García Arenas, L.F. Vilches, J. Vale, A. Gimenez, J.C. Ballesteros, C. Fernández-Pereira, Use of FGD gypsum in fire resistant panels, Waste Manage. 30 (2010) 1123–1129.
[38] Ligia Tiruta-Barna, Enrico Benetto, Yves Perrodin, Environmental impact and risk assessment of mineral wastes reuse strategies: review and critical analysis of approaches and applications, Resour. Conserv. Recy. 50 (2007) 351–379.
[39] X. Gao, W. Wang, T. Ye, F. Wang, Y. Lan, Utilization of washed MSWI fly ash as partial cement substitute with the addition of dithiocarbamic chelate, J. Environ. Manage. 88 (2008) 293–299.